Title	Electron diffraction study of the sillenites Bi_<12>SiO_<20>, Bi_<25>FeO_<39> and Bi_<25>InO_<39> : Evidence of short-range ordering of oxygen-vacancies in the trivalent sillenites
Author(s)	Scurti, Craig A., Auvray, Nicolas, Lufaso, Michael W., Takeda, Seiji, Kohno, Hideo, Arenas, D. J.
Citation	AIP Advances, 4(8): 087125-1-087125-10
Date of issue	2014-08
URL	http://hdl.handle.net/10173/1450
Rights	
Text version	publisher

Electron diffraction study of the sillenites Bi$_{12}$SiO$_{20}$, Bi$_{25}$FeO$_{39}$ and Bi$_{25}$InO$_{39}$: Evidence of short-range ordering of oxygen-vacancies in the trivalent sillenites

Craig A. Scurti,[1] Nicolas Auvray,[1,2] Michael W. Lufaso,[3] Seiji Takeda,[4] Hideo Kohno,[5] and D. J. Arenas[1]

[1]*Department of Physics, University of North Florida, Jacksonville, FL 32224 USA*
[2]*Laboratoire de Nanotechnologie et d'Instrumentation Optique - UMR CNRS 6279, Université Technologie de Troyes, 12 rue Marie Curie, Troyes 10010, France*
[3]*Department of Chemistry, University of North Florida, Jacksonville, FL 32224 USA*
[4]*The Institute of Scientific and Industrial Research, Osaka University, 8-1 Mihogaoka, Ibaraki, Osaka 567-0047, Japan*
[5]*School of Environmental Science and Engineering, Kochi University of Technology, Tosayamada, Kami, Kochi 782-8502 Japan*

We present an electron diffraction study of three sillenites, Bi$_{12}$SiO$_{20}$, Bi$_{25}$FeO$_{39}$, and Bi$_{25}$InO$_{39}$ synthesized using the solid-state method. We explore a hypothesis, inspired by optical studies in the literature, that suggests that trivalent sillenites have additional disorder not present in the tetravalent compounds. Electron diffraction patterns of Bi$_{25}$FeO$_{39}$ and Bi$_{25}$InO$_{39}$ show streaks that confirm deviations from the ideal sillenite structure. Multi-slice simulations of electron-diffraction patterns are presented for different perturbations to the sillenite structure - partial substitution of the M site by Bi^{3+}, random and ordered oxygen-vacancies, and a frozen-phonon model. Although comparison of experimental data to simulations cannot be conclusive, we consider the streaks as evidence of short-range ordered oxygen-vacancies. *© 2014 Author(s). All article content, except where otherwise noted, is licensed under a Creative Commons Attribution 3.0 Unported License.* [http://dx.doi.org/10.1063/1.4893341]

I. INTRODUCTION

Sillenites are technologically-interesting due to their photo-refractive,[1–4] piezo-electric,[5] electro-optical,[6–10] and elasto-optical properties.[11,12] The last decade has witnessed an increase in the study of these compounds for photocatalysis and novel applications.[13–17] The physical and electronic structure of sillenites remains important and continues to motivate synthesis,[18–22] optical,[23–25] first principles,[26–28] dielectric,[29] magnetism,[30] and high-pressure studies.[31,32]

Figure 1 shows a representative sillenite structure. The structure belongs to the *I*23 space group and is described by a Bi-O framework connecting isolated oxygen-tetrahedra. The center of each tetrahedron is labelled as the M site and houses metal cations. The oxygens in the tetrahedra are labelled O(3). There are two symmetry-differing oxygen sites labelled as O(1) and O(2) that make up the Bi-O framework outside the tetrahedra. The sillenite structure is exclusive to bismuth oxygen compounds and is described by the meta-stable parent-compound γ-Bi$_2$O$_3$ which houses the Bi^{3+} ion in the center of the tetrahedron.[33] In the sillenites, Bi$_{12}$SiO$_{20}$ and Bi$_{12}$GeO$_{20}$, the sillenite structure is stabilized by fully replacing the Bi^{3+} ion by small tetravalent ions. These two tetravalent sillenites have the simplest structure of all sillenites and their structure will be referred to as the ideal structure. In Bi$_{25}$FeO$_{39}$ and Bi$_{25}$InO$_{39}$ the structure is stabilized by trivalent ions; but there are two important differences in the stoichiometry. First, the M site is equally occupied by M^{3+} and Bi^{3+} ions. And second, the tetrahedra with a Bi^{3+} ion have an oxygen vacancy which makes room for the 6s^2 lone pair of bismuth.[19] Divalent, pentavalent, and even hexavalent compounds can also be synthesized,
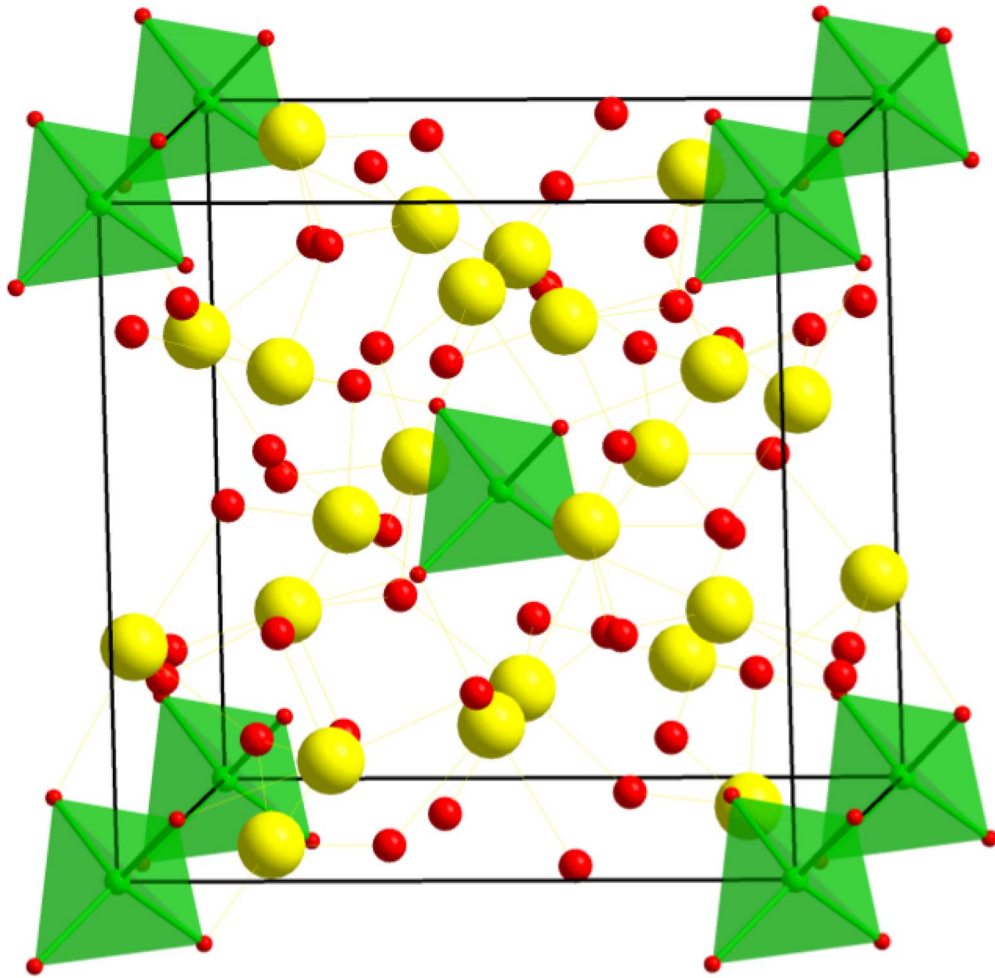
FIG. 1. A representative sillenite structure. The structure is stabilized from the parent compound by an *M* cation in the center of the tetrahedra (i.e. Si^{4+}, Ti^{4+}, Fe^{3+}, In^{3+}). The tetrahedra (green) at the corners and center of the unit cell are connected by a Bi-O framework (Bi: yellow, O: red).

and the partial occupancy of the M site varies for different valences. More detail about the structure can be found in references 19, 34.

The stoichiometry and structures described above correspond to the models proposed by Valant in 2002.[19] This comprehensive model of sillenites is dependent on the conclusion by Radaev and Simonov that the parent γ-Bi_2O_3 compound houses Bi^{3+} in the center of the tetrahedron,[33,35,36] and that it is unlikely that Bi^{5+} partially occupies the M site of divalent and trivalent sillenites.[19] Some recent publications instead claim a $Bi_{25}FeO_{40}$ chemical formula for the iron sillenite,[17,22] and some justify the stoichiometry by citing work from Craig and Stephenson.[37] Unfortunately, some of the publications claiming the $Bi_{25}FeO_{40}$ chemical formula[17,22,38] do not comment on the more recent, heavily cited, and comprehensive model of sillenites that uses Bi^{3+} partial occupation of the M site.[19] The controversy is further complicated by the fact that some of the studies quoting the $Bi_{25}FeO_{40}$ formula use the hydrothermal growth method.[22] In our study we used the solid-state growth method; therefore, we use the $Bi_{25}FeO_{39}$ chemical formula due to the lack of experimental evidence for the stabilization of Bi^{5+} in systems grown by the solid-state method.

As new sillenites are synthesized, it is important to understand their electronic and structural properties and determine their efficiency in applications such as nonlinear optics and photocatalysis. A recent Raman spectroscopy study showed that the vibrational modes have considerably larger widths in trivalent compounds than in tetravalent compounds.[25] The wider distribution of resonant

frequencies suggests differing force constants across neighbouring unit cells. Since the X-ray spectra of the trivalent sillenites do not show deviations from the ideal structure, whichever structural deviation is present must average to the ideal structure for a large number of unit cells. Therefore, it was suggested that inhomogeneous disorder, or statistical deviations from the average structure, is responsible for the wider distribution of resonant frequencies.

In the present work, an electron diffraction study of sillenite crystals was undertaken to investigate the disorder of the trivalent compounds. Our results show that the ED patterns of $Bi_{12}SiO_{20}$ and the new trivalent sillenites, $Bi_{25}FeO_{39}$ and $Bi_{25}InO_{39}$, agreed with an average structure in the $I23$ space group. However, $Bi_{25}FeO_{39}$ and $Bi_{25}InO_{39}$ show streaks in their ED patterns that were not observed for the tetravalent $Bi_{12}SiO_{20}$. The measurements prove a deviation of the trivalent sillenites from the ideal sillenite structure and corroborate the hypothesis from previous optical studies.[25] Various structural models were explored using multi-slice simulations of the ED patterns. We present simulations involving random substitutions of the M site by Bi^{3+}, random and ordered oxygen-vacancies, and frozen phonons. Quantitative comparisons between the simulations and experimental ED patterns are difficult and should not be considered conclusive; however, the results suggest that short-range ordered oxygen-vacancies are responsible for the streaking in the ED patterns.

II. EXPERIMENTAL PROCEDURES

The samples were synthesized by solid-state reaction in air using stoichiometrically-weighed high purity oxides. Reactants were ground using an agate mortar and pestle under acetone, then initially heated at 700°C in a high-form alumina crucible. Multiple heating cycles, with intermediate grinding, were conducted at 750°C.

Samples were analyzed by X-ray powder diffraction using a Rigaku Ultima III X-ray diffractometer with Cu Kα radiation. Equilibrium was assumed when no shift or change in intensity of the weakest peaks from the XRD pattern was observed. The structures of the single phase compounds were refined using the Rietveld technique and the FULLPROF software program. The same physical samples as the previous Raman study were used.[25] The SEM images were taken using a JEOL JSM5510. Crystallites on the order of 1-10 μm were detected for all samples.

Transmission electron microscopy measurements were carried using a JEOL JEM 2010 TEM. The operating voltage of the TEM, 160 kV, was similar to those used in other reports studying streaking of different systems.[39–41] 30-50 crystallites were explored for each compound. The crystallites were ground and placed on a Cu microgrid with a carbon supporting film. A silicon crystal was used for calibration. The rotation limit of the TEM was 20 degrees; therefore, different crystallites had to be measured to be able to view the compound from different zone-axes. We did not observe any secondary phases from the TEM results. The streaks in the ED pattern were weak and their intensities varied among crystallites. Furthermore, the exposure times required to see the streaks were 4 to 8 times larger than the usual time to collect a simple ED pattern. These experimental difficulties in observing streaks have been reported in other systems with large unit cells.[41] Multi-slice calculations of the electron diffraction patterns were carried using the MacTempas commercial software program. Slices in the order of 1 Å and sample thicknesses of 100 Å were used for the simulations (unless otherwise noted).

III. RESULTS AND DISCUSSION

Figure 2 shows representative electron diffraction images for $Bi_{12}SiO_{20}$, $Bi_{25}FeO_{39}$, and $Bi_{25}InO_{39}$ along the major zone axes. The kinematical approximation predicts bcc selection rules where the allowed reciprocal vectors (h, k, l) must have indices adding up to an even number. Multiple scattering, however, can frequently result in kinematically forbidden reflections. Our experimental ED patterns in the major zone axes did not show any forbidden reflection spots. Our multi-slice calculations for the ideal sillenite structures also did not show multiple scattering and forbidden reflection spots.

The lattice parameters were consistent with those measured with X-ray analysis.[25] Figure 3 shows the ED patterns of $Bi_{25}InO_{39}$ along the [210], [731], and [751] zone axes. All figures
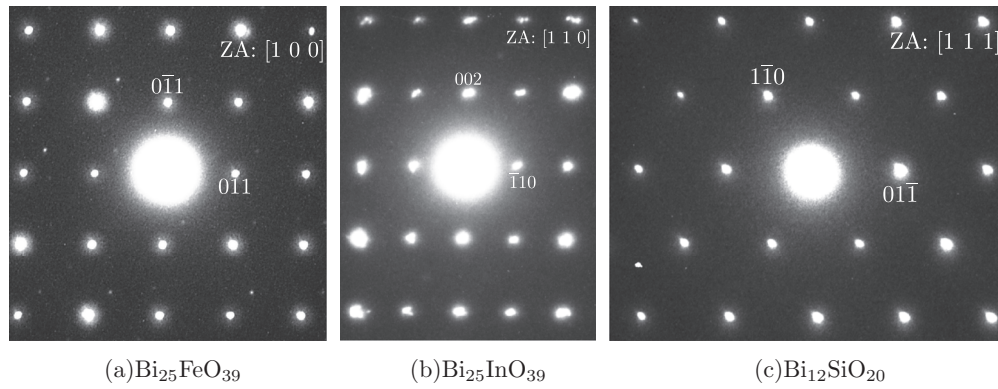
FIG. 2. Representative electron diffraction patterns of $Bi_{25}FeO_{39}$, $Bi_{25}InO_{39}$, and $Bi_{12}SiO_{20}$ for the [100], [110], and [111] zone axes, respectively.
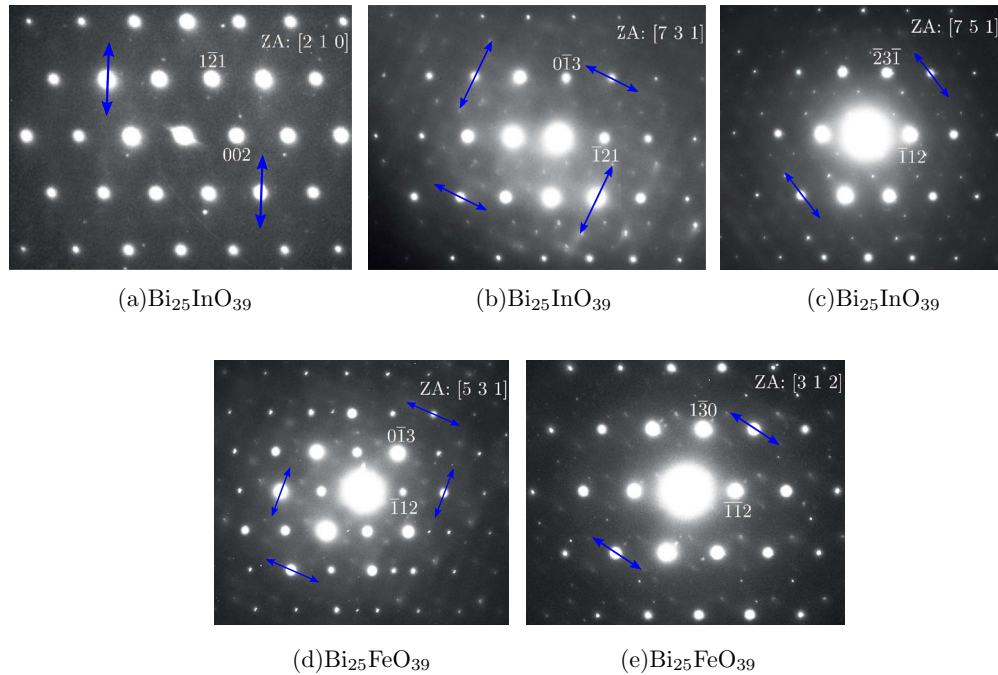

FIG. 3. Streaks in the ED patterns of $Bi_{25}InO_{39}$ (a-c) and $Bi_{25}FeO_{39}$ (d-e). The streaks were observed at multiple zone-axes; representative patterns for $Bi_{25}InO_{39}$ are shown for the [210], [731], and [751] zone axes; and [531] and [312] for $Bi_{25}FeO_{39}$. Blue arrows denoting the directions of the streaks were added as an aid to the eye. Each figure corresponds to a different crystal. The streaks were in different reciprocal lattice directions for different crystallites.

correspond to different crystallites and they showed streaks in different directions. For example, weak streaks appear in the (-1,2,0) reciprocal-space direction for the crystallite viewed along the [210] zone axis, and in the (-1,0,7) direction for the one viewed along the [731] zone axis. $Bi_{25}FeO_{39}$ also showed streaks in some of its ED patterns (Fig. 3). Several crystallites, many viewed along high index zone axes, were measured for $Bi_{12}SiO_{20}$ but no streaks were ever observed. Furthermore, some of the streaks also showed weak reflection spots associated with an elongation of the unit cell.

The appearance of streaks in the trivalent sillenites, and their absence in the $Bi_{12}SiO_{20}$ compound, is an observation of a deviation from the ideal sillenite structure. In other words, the trivalent sillenites have significant structural differences compared to the tetravalent sillenites. There are different perturbations to the ideal structure that could result in intensity streaks in an ED pattern as those in our experimental data (Figures 2 and 3). The multiple possibilities hampers the attribution
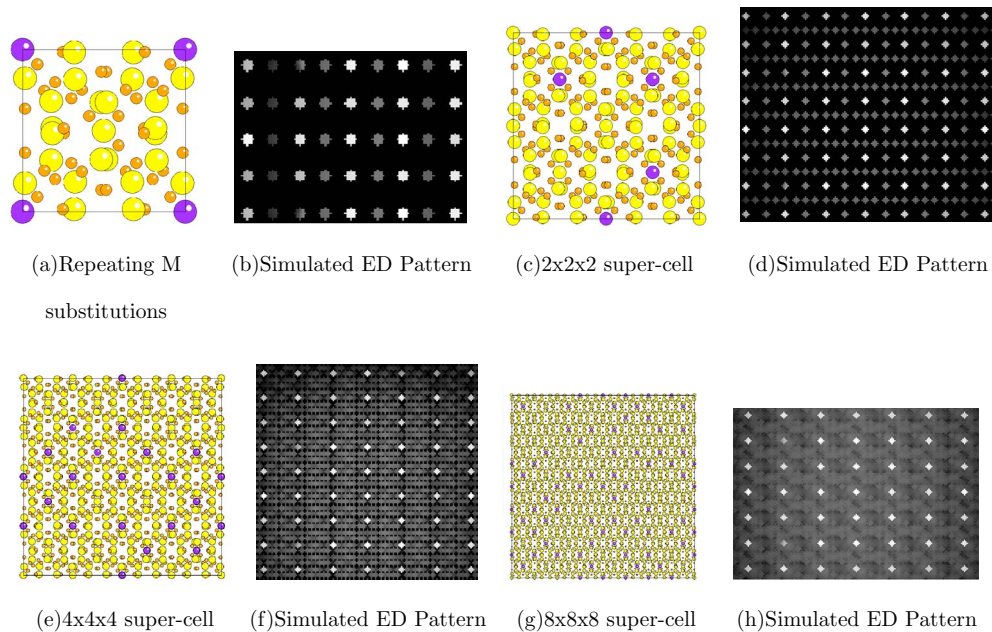
(a)Repeating M substitutions   (b)Simulated ED Pattern   (c)2x2x2 super-cell   (d)Simulated ED Pattern

(e)4x4x4 super-cell   (f)Simulated ED Pattern   (g)8x8x8 super-cell   (h)Simulated ED Pattern

FIG. 4. Multi-slice ED simulations of models involving substitutions of the M site. Figure A shows the [011] diffraction pattern of a model where Bi^{3+} always occupies the center of the unit cell. Figures (b)-(d) show super-cells with increasing size where the occupation of the M site by Bi^{3+} or M^{3+} was randomly generated. The results show that an $8\times8\times8$ super-cell with random substitutions is sufficient to satisfy the bcc selection rules.

of the streaks to a particular deviation. In the following sections, we discuss a few physical models that could result in the streaks shown in our experimental data.

A. Bismuth substitutions in the M site

One important difference in the suggested stoichiometry of trivalent sillenites is the partial occupation of the M site by Bi^{3+} cations.[19] The distribution of Bi^{3+} and M^{3+} cations in the M site must be random. Otherwise, the bcc selection rules will not be satisfied since the scattered wavefunctions from both atoms would not cancel completely due to the difference in scattering amplitude. Since our data did not show multiple-scattering and the bcc selection rules were satisfied, it is interesting to explore how the partial occupation of the M site in trivalent sillenites can still yield a bcc ED-pattern. Figure 4 shows a set of multi-slice calculations exploring M substitutions. Figure 4(a) shows a simple unit cell where In^{3+} always occupies the edges and Bi^{3+} always occupies the center. It is obvious that the selection rules for bcc would be broken. The multi-slice calculations, Figure 4(b), agree with the simple prediction and show reflection spots forbidden for a bcc structure.

The random occupation of the M site was modelled in the multi-slice calculation by building larger super-cells. Figures 4(c), 4(e) and 4(g) show three super-cells of increasing size; the occupancy of each M site was randomly generated with equal probabilities of occupancies by Bi^{3+} and In^{3+}. Figure 4 shows representative electron diffraction patterns, viewed along the [011] zone-axis in this case, for each super-cell. The results show that an $8\times8\times8$ super-cell with random M site occupation is sufficient to satisfy the bcc selection-rules. Due to the large size of each unit cell (66 atoms), $8\times8\times8$ was the largest super-cell (33792 atoms) used in our calculations. Checking the satisfaction of the bcc selection rules was useful to justify the limited-size super-cell.

The multi-slice calculations using the largest super-cell shows only the reflection spots predicted for bcc, but it also shows strong diffuse scattering in the center of the ED pattern. Unfortunately, there are at least two difficulties in using the intensity of the diffuse scattering for comparison to experimental results. One, the exposure time and the film responsiveness are not modelled quantitatively. And two, the intensity of the diffuse scattering is dependent on the thickness of the
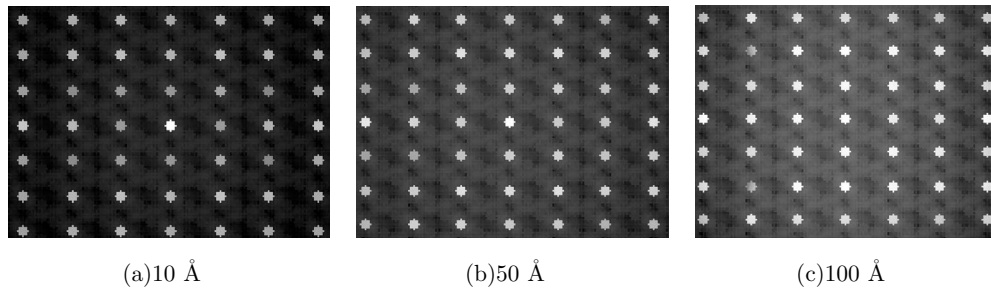
(a)10 Å	(b)50 Å	(c)100 Å

FIG. 5. Multi-slice ED simulations of an 8×8×8 super-cell with random M occupancy. ED simulation for different crystal-thickness are shown. The simulations show that the intensity of the central diffuse scattering is heavily dependent on the thickness of the crystal.

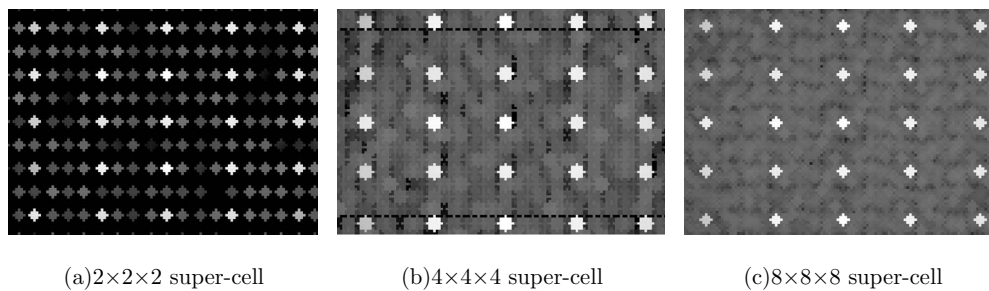|		
(a)2×2×2 super-cell	(b)4×4×4 super-cell	(c)8×8×8 super-cell

FIG. 6. Multi-slice [011] ED simulations of increasing-size super-cells with random O(3) vacancies.

crystal. Figure 5 shows multi-slice calculations for the 8×8×8 super-cell in Figure 4(g), and the simulations shows that the strength of the central diffuse scattering strongly depends on the crystal thickness.

B. Random and ordered oxygen-vacancies

The stoichiometry of trivalent sillenites suggested by Valant predicts an oxygen vacancy in each tetrahedron whose center is occupied by Bi^{3+}. The lone pair of Bi^{3+} requires an oxygen vacancy in the surrounding tetrahedron. However, it is random which of the four oxygen-sites in the tetrahedron is vacant. Multi-slice calculations with various sized super-cells were carried to study the effect of oxygen vacancies. An otherwise perfect sillenite structure, without random M substitutions, was built; then each O(3) oxygen-site was given an 1/8 probability of having a vacancy. Similar to the M substitution simulations, O(3) vacancies must be random or else the bcc selection rules were broken. Figure 6 shows the electron diffraction simulations for increasing-size super-cells and show that an 8×8×8 super-cell was sufficient to predict the bcc reflection spots. Simulations involving different thicknesses, not shown, also showed that the intensity of the central diffuse scattering depended heavily on the crystal thickness. All the qualitative results were identical for a model where the oxygen vacancy could also occur in the Bi-O framework.

Ordered periodic vacancies is one mechanism to create a modulation of the charge density and could result in streaks in the ED pattern. Short-range ordering of oxygen-vacancies, as chains of vacancies, have been attributed as responsible for diffuse streaks in many systems; these include oxygen-deficient stoichiometries of the superconductors $YBa_2Cu_2O_{7-\delta}$,[41,42] and $Nd_{2-x}Ce_xCuO_{4-y}$;[43] and the perovskite $CaFe_xTi_{1-x}O_{3-x/2}$.[39,40] Although there are different types of geometries possible for the ordering of oxygen-vacancies, and their existence has been shown by streaks in electron diffraction patterns,[44,45] in this report we concentrate on a simple chain geometry. Also, we emphasize that we did not model the lattice relaxation of the atoms near the vacancy; the simple approximation is physically based on the model that the lone pair of Bi^{3+} fills the vacancy.

(a)[001]   (b)[010]   (c)[100]

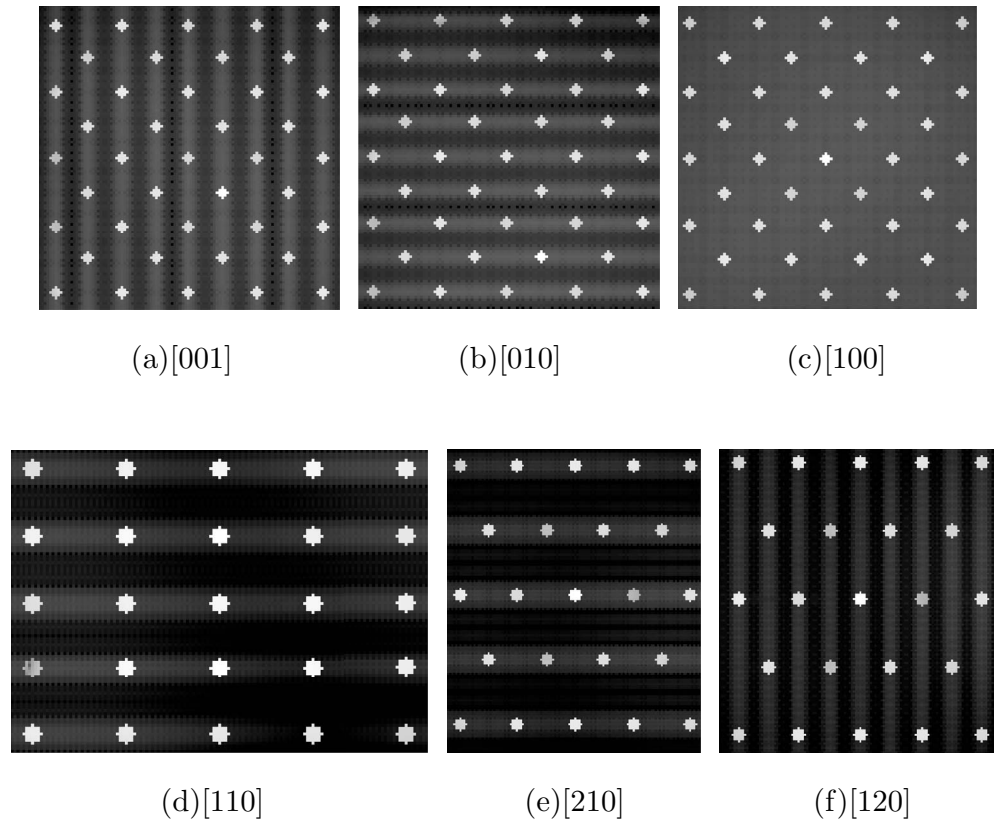(d)[110]   (e)[210]   (f)[120]

FIG. 7. Multi-slice simulations of electron diffraction patterns for a chain of oxygen vacancies in the [100] direction of the sillenite crystal. An 8×8×8 super-cell was used. Note that the streaks can be viewed along many zone-axes and only disappear when viewing the crystal along the direction of the chain in real space.

Figure 7 shows multi-slice simulations for an 8×8×8 sillenite super-cell with a chain of 4 oxygen vacancies in the 100 direction of the crystal. The simulation results in well defined streaks. An important result is that the streaks can be viewed along many zone-axes of the crystal directions. As expected, the streaks are not visible when viewing the crystal along the oxygen-vacancy chain (Fig. 8(d)). Different directions of the oxygen-vacancy chain, 110 and 111, were used in the simulations and the same qualitative results were obtained.

A more realistic model would include the short oxygen-vacancy chain inside a super-cell where all the other O(3) sites were randomly vacated. Unfortunately, it is not possible to observe the streaks caused by the chains due to the strong central diffused scattering caused by the random vacancies. The difficulties in quantitative comparisons between the simulations and experiment, especially for such a large unit cell, negates the need to try to find the exact conditions for the crystal for which streaks could be observed even among the central diffuse scattering. Our main point is that short-range ordering of oxygen vacancies in sillenites would result in streaks in the ED pattern. As a final note, an 8×8×8 super-cell with one oxygen vacancy was also simulated and the ED pattern did not show streaks; ordering was necessary to result in streaks.

C. Frozen phonon model

Another possibility to modulate the charge density is to periodically displace atoms from their ideal position. There are two possibilities: a displacement in the direction of the modulation (longitudinal) and a displacement perpendicular to the direction of the modulation (transverse). A physical candidate for this type of modulation is a frozen-phonon mode (FP); a phonon mode from a higher temperature and higher-symmetry phase that freezes during the cool-down portion
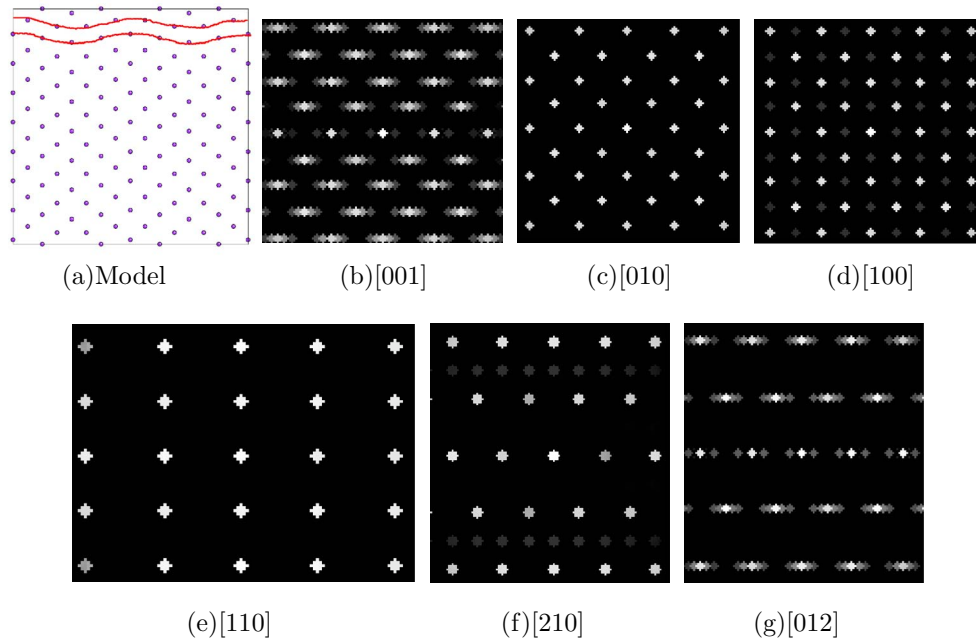
FIG. 8. Multi-slice simulation of electron diffraction pattern for a frozen transverse-phonon. Figure (a) shows a crystal model where each M atom is displaced by an amount modulated in the 100 crystal direction. The magnitude of the displacements were exaggerated for (a) as an aid to the eye. Note that the streaks are weak for directions that are not perpendicular to the phonon wave-vector. Also note that the streaks appear in the 100 k-space direction and that viewing the crystal along the modulation results in reflection spots forbidden for the bcc geometry.

of the solid-state synthesis. Unfortunately, there are no reports in the literature on the structural properties of $Bi_{25}FeO_{39}$ and $Bi_{25}InO_{39}$ at higher temperatures. The FP model should still be explored since the streaks in ED patterns have been attributed to frozen-phonons in other systems.[46,47] Figure 8(a) shows an example of a super-cell where the atoms are displaced by a periodic amount; in this case, a transverse modulation in the 100 direction where the displacement of the atoms was greatly exaggerated as an aid to the eye. In our multi-slice simulations, we used a wavelength four times as large as the unit-cell of the sillenite and a displacement of 0.01 Å.

At first look, there is a major qualitative difference between the frozen-phonon multi-slice simulations and our experimental data. The FP simulated images in Figure 8 show satellite spots only near the main reflection spots. It is clear that only the first satellite spots appear in the simulation due to the perfectly sinusoidal modulation. The simulations of the oxygen-vacancy chain gave more elongated streaks and seemed to agree better with the data. The qualitative agreement is better for the oxygen-vacancy model and suggests the model's validity above the frozen phonon model. However, it should be argued that the comparison between the simulations of these two models and the experimental data is not 100 percent conclusive. One may argue that the extra satellite spots, near the main reflection spots, generated by the FP model may look like streaks in the experimental ED pattern if the satellite spots are weak. Also, a sinusoidal perturbation with a limited length may result in longer elongations.

A stronger evidence that the ordered oxygen-vacancies model agrees better with experiment is the appearance of streaks in different k-space directions and that the streaks are viewed along many zone-axes. In the frozen-phonon simulations the streaks tend to be visible only when viewing the crystal perpendicular to the direction of the modulation and perpendicular to the displacements. Also, the streaks have well defined directions in k-space that are related to the direction of the modulation in real space. Our experimental data shows streaks for ED patterns viewed along many zone-axes and with different directions in k-space. As a reminder, TEM sample-holders can only be rotated by a limited amount and every crystallite measured could only be studied in a small range of incoming angles. If the streaks in our experimental data were due to frozen-phonons then we have

viewed crystallites with frozen-phonons in different directions; and, we were fortunate to be able to view the crystallite at a zone-axis perpendicular to the modulation. It is therefore more likely that we are viewing streaks resulting from ordering of oxygen-vacancies that can appear when viewed along different zone-axes.

D. Relevance to previous optical studies and future work

In a recent Raman spectroscopy study,[25] it was shown that the width of the Raman modes was larger for the trivalent compounds than for the tetravalent compounds. It was suggested that inhomogeneous disorder, that is deviations from the average structure that differ from one unit cell to another, was responsible for the wider distribution of resonant frequencies. Oxygen-vacancies, ordered or disordered, would also result in variations across unit cells of the force constants and the vibrational resonant frequencies. At this point it is not clear whether the same disorder is responsible for the large phonon widths observed in the Raman and the streaks observed in the ED patterns. However, the results are consistent. And the consistency is strengthened by the fact that the streaks were missing in the tetravalent $Bi_{12}SiO_{20}$ compound.

Our assignment of the streaks to the ordering of oxygen-vacancies is also contingent on the validity of the $Bi_{25}M^{3+}O_{39}$ stoichiometry model. The reader is suggested to read the work by Valant and Radaev to justify the model of Bi^{3+} occupying the center of the tetrahedron.[19] The stoichiometry controversy needs to be settled, however, because Bi^{5+} occupation of the M site could also result in streaks due to charge ordered states similar to those observed in $La_{1-x}Sr_xFeO_3$.[48] New neutron scattering, or synchrotron X-ray, studies would be interesting in exploring different models of the deviation in trivalent sillenites. Finally, electron diffraction of $Bi_{25}InO_{39}$ single crystals would provide a systematic study capable of assigning the ordering of oxygen-vacancies to a particular geometry.

IV. CONCLUSIONS

The electron diffraction patterns of three sillenite compounds have been investigated. Streaks in the ED pattern of $Bi_{25}FeO_{39}$ and $Bi_{25}InO_{39}$, not observed in $Bi_{12}SiO_{20}$, confirm a deviation from the average structure. The results are consistent with previous optical studies. Multi-slice simulations of different models were used to try to reproduce the ED patterns of the trivalent sillenites. Although quantitative comparisons are difficult, the results suggest that the streaks are caused by short-range ordering of oxygen-vacancies. Future measurements using other techniques, such as neutron scattering, may bring more information to the origin of the modulation. Regardless, the results are interesting because many systems involving ordering of oxygen-vacancies, or charge ordered states, display interesting physics.[41,42,45,48]

[1] S. L. Sochava, K. Buse, and E. Krätzig, Phys. Rev. B **51**, 4684 (1995).

[2] H. C. Pedersen, D. J. Webb, and P. M. Johansen, J. Opt. Soc. Am. B **15**, 2573 (1998).

[3] V. Jerez, I. de Oliveira, and J. Frejlich, Journal of Applied Physics **109**, 024901 (2011).

[4] J. Ricardo, M. Muramatsu, F. Palcios, M. Gesualdi, J. Valin, and M. A. P. Lopez, Optics and Lasers in Engineering (2013).

[5] A. Ballman, H. Brown, P. Tien, and R. Martin, Journal of Crystal Growth **20**, 251 (1973).

[6] V. Chmyrev, V. Skorikov, and E. Larina, Inorganic Materials **42**, 381 (2006).

[7] A. Efremidis, N. Deliolanis, C. Manolikas, and E. Vanidhis, Applied Physics B: Lasers and Optics **95**, 467 (2009).

[8] I. de Oliveira, T. dos Santos, J. Carvalho, and J. Frejlich, Applied Physics B: Lasers and Optics **105**, 301 (2011).

[9] A. Kamshilin, A. Grachev, S. Golik, R. Romashko, and Y. Kulchin, Applied Physics B **106**, 899 (2012).

[10] A. Moura, A. Canabarro, W. Soares, E. de Lima, J. Carvalho, and P. dos Santos, Optics Communications **295**, 197 (2013).

[11] E. L. Venturini, E. G. Spencer, and A. A. Ballman, Journal of Applied Physics **40**, 1622 (1969).

[12] M. Peltier and F. Micheron, Journal of Applied Physics **48**, 3683 (1977).

[13] W. Yao, H. Wang, X. Xu, J. Zhou, X. Yang, Y. Zhang, S. Shang, and M. Wang, Chemical Physics Letters **377**, 501 (2003).

[14] W. F. Yao, H. Wang, X. H. Xu, X. F. Cheng, J. Huang, S. X. Shang, X. N. Yang, and M. Wang, Applied Catalysis A: General **243**, 185 (2003).

[15] X. Lin, F. Huang, W. Wang, Y. Xia, Y. Wang, M. Liu, and J. Shi, Catalysis Communications **9**, 572 (2008).

[16] B.-H. Kim, T.-H. Lim, J.-W. Roh, S.-G. Lee, C. Ju, S. Park, S. Hong, and G. Lee, Reaction Kinetics, Mechanisms and Catalysis **99**, 217 (2010).

[17] A. Sun, H. Chen, C. Song, F. Jiang, X. Wang, and Y. Fu, RSC Advances **3**, 4332 (2013).

[18] M. Valant and D. Suvorov, Journal of the American Ceramic Society **84**, 2900 (2001).

[19] M. Valant and D. Suvorov, Chemistry of Materials **14**, 3471 (2002).

[20] M. Valant and D. Suvorov, Journal of the American Ceramic Society **85**, 355 (2002).

[21] H. Sekhar and D. N. Rao, Journal of Materials Science: Materials in Electronics , 1 (2013).

[22] R. Köferstein, T. Buttlar, and S. G. Ebbinghaus, Journal of Solid State Chemistry (2014).

[23] T. Milenov, P. Rafailov, C. Thomsen, A. Egorysheva, R. Titorenkova, B. Kostova, and V. Skorikov, Optical Materials **33**, 1573 (2011).

[24] H. Sekhar, P. P. Kiran, and D. N. Rao, Materials Chemistry and Physics **130**, 113 (2011).

[25] D. J. Arenas, T. Jegorel, C. Knab, L. V. Gasparov, C. Martin, D. M. Pajerowski, H. Kohno, and M. W. Lufaso, Phys. Rev. B **86**, 144116 (2012).

[26] A. F. Lima, S. A. S. Farias, and M. V. Lalic, Journal of Applied Physics **110**, 083705 (2011).

[27] H. Deng, W. Hao, and H. Xu, Rare Metals **30**, 135 (2011).

[28] S. A. Farias and J. B. L. Martins, Chemical Physics Letters **533**, 78 (2012).

[29] Y. Hu and D. C. Sinclair, Chemistry of Materials **25**, 48 (2012).

[30] L. A. S. de Oliveira, J. P. Sinnecker, M. D. Vieira, and A. Penton-Madrigal, Journal of Applied Physics **107**, 09D907 (2010).

[31] R. Rao, A. B. Garg, and T. Sakuntala, Journal of Applied Physics **108**, 083508 (2010).

[32] L. Wiehl, A. Friedrich, E. Hausshl, W. Morgenroth, A. Grzechnik, K. Friese, B. Winkler, K. Refson, and V. Milman, Journal of Physics: Condensed Matter **22**, 505401 (2010).

[33] S. Radaev, V. Simonov, and Y. F. Kargin, Acta Crystallographica Section B: Structural Science **48**, 604 (1992).

[34] W. Wojdowski, Physica Status Solidi (B) **130**, 121 (1985).

[35] S. F. Radaev, L. A. Muradyan, and V. I. Simonov, Acta Crystallographica Section B **47**, 1 (1991).

[36] V. Radaev and S. F. Simonov, Kristallografiya **37**, 914 (1992).

[37] D. Craig and N. Stephenson, Journal of Solid State Chemistry **15**, 1 (1975).

[38] Y. Sun, X. Xiong, Z. Xia, H. Liu, Y. Zhou, M. Luo, and C. Wang, Ceramics International (2012).

[39] A. I. Becerro, F. Langenhorst, R. J. Angel, S. Marion, C. A. McCammon, and F. Seifert, Physical Chemistry Chemical Physics **2**, 3933 (2000).

[40] C. McCammon, A. Becerro, F. Langenhorst, R. Angel, S. Marion, and F. Seifert, Journal of Physics: Condensed Matter **12**, 2969 (2000).

[41] C. Hou, A. Manthiram, L. Rabenberg, and J. Goodenough, Journal of Materials Research **5**, 9 (1990).

[42] D. Werder, C. Chen, R. Cava, and B. Batlogg, Physical Review B **37**, 2317 (1988).

[43] T. Williams, Y. Maeno, I. Mangelschots, A. Reller, and G. Bednorz, Physica C: Superconductivity **161**, 331 (1989).

[44] J. Castles, J. Cowley, and A. Spargo, Acta Crystallographica Section A: Crystal Physics, Diffraction, Theoretical and General Crystallography **27**, 376 (1971).

[45] C. Chaillout and J. Remeika, Solid state communications **56**, 833 (1985).

[46] R. Withers, Progress in Crystal Growth and Characterization **18**, 139 (1989).

[47] G. Van Tendeloo, J. Van Landuyt, and S. Amelinckx, Physica Status Solidi (A) **33**, 723 (1976).

[48] J. Li, Y. Matsui, S. Park, and Y. Tokura, Physical review letters **79**, 297 (1997).